CRYSTAL GROWTH & DESIGN

pubs.acs.org/crystal

Article

Structural and CO_2 Capture Properties of Ethylenediamine-Modified HKUST-1 Metal−Organic Framework

Nika Vrtovec,[▽] Matjaž Mazaj,*[,▽] Gianpiero Buscarino, Angela Terracina, Simonpietro Agnello, Iztok Arčon, Janez Kovač, and Nataša Zabukovec Logar[▽]

Cite This: *Cryst. Growth Des.* 2020, 20, 5455−5465

Read Online

ACCESS | Metrics & More | Article Recommendations | Supporting Information

ABSTRACT: The high structural and compositional flexibility of metal−organic frameworks (MOFs) shows their great potential for CO_2 capture and utilization in accordance with the environmental guidelines of low-carbon technology developments. HKUST-1 as one of the most intensively studied representatives of MOFs for such purposes excels because of its simplicity of production and high ability to tune its intrinsic properties by various functionalization processes. In the present work, ethylenediamine functionalization was performed for the first time in order to thoroughly investigate the amine sorption sites' impact on the CO_2 capture performance of HKUST-1. The placement of ethylenediamine moieties on Cu^{2+} free-metal sites has been examined in detail and confirmed by using various spectroscopic techniques such as Fourier transform infrared spectroscopy, electron paramagnetic resonance, Raman, and Cu K-edge extended X-ray absorption fine structure/X-ray absorption near edge structure. N_2 and CO_2 sorption tests have proven that the functionalization reduces both the specific surface area and the CO_2 sorption capacity, but on the other hand, it increases the binding energy by 85% (from −20.3 kJ/mol to −36.8 kJ/mol) and CO_2/N_2 selectivity at 0.15/0.85 bar by 100% and notably improves the kinetics of adsorption in comparison to the pristine HKUST-1 material.

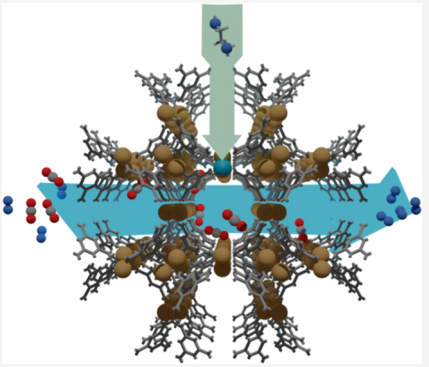

INTRODUCTION

Postcombustion CO_2 capture (PCC) is a well-established method of carbon capture and storage (CCS) technology enabling retrofitting at a point source and sustainability of the combustion process. Typically, the flue gas is composed of 75% N_2, 15% CO_2, 5% H_2O, and a small amount of SO_x and NO_x. The conventional PCC process based on chemisorption in monoethanolamine solutions suffers drawbacks of a large energy penalty for sorbent regeneration, thermal and oxidative amine degradation, and corrosion issues.[1−9] Therefore, the alternative technology based on physisorption on solid sorbents, which to a major extent surpasses the above-mentioned drawbacks, has been intensively studied. Adsorbents with efficient CO_2 capture performances must possess several desirable characteristics such as high adsorption capacity at low partial pressure (p/p_o = 0.1−0.2), high sorption selectivity and chemical resistivity over accompanying components commonly present in postcombustion systems (e.g., N_2, H_2O, SO_x, and NO_x), high rates of adsorption/desorption kinetics, energy-efficient regeneration, structure stability, and low production cost.[3,5,10−13]

Recently, several materials have been developed for CO_2 capture, based on physisorption on solid adsorbents, e.g., porous organic polymers, covalent organic framework, activated carbon, zeolites, and metal−organic framework (MOFs).[3,5,14] Because of their wide range of potential applications, high working capacity, and tuneability of sorption properties, MOFs are one of the most promising candidates for CO_2 capture.[4,8−11,14,15] Targeted properties of MOFs can be optimized either by rational design using appropriate starting precursors or postsynthetically by the chemical introduction of functional groups on metal centers or ligands.[4,11,16−18] In that manner, numerous approaches have been used to tune the guest−host interactions for CO_2 molecules for example by inclusion of amine, halide, or hydroxyl groups.[19−21] The proven technology of amine scrubbing in the gas−liquid interface could potentially be transferred to gas−solid adsorbents. It has been demonstrated that the incorporation of nitrogen-based groups at active metal sites presents a simple method for improving the capture and separation capabilities of porous solids at ambient conditions, in particular, selectivity for CO_2.[22]

Ethylenediamine (ED), as a low molecular weight molecule with a relatively small kinetic diameter containing terminal amino groups, which can interact with open metal sites or CO_2

Received: May 15, 2020
Revised: July 10, 2020
Published: July 10, 2020

molecules, was used as a functionalizing agent in several studies.[15,19,23−26] Long and co-workers have described that the incorporation of ED molecules to Cu-BTTri open metal sites exhibits a higher uptake of CO_2 at low pressures and a clear enhancement of isosteric heat of adsorption in comparison to the parent material.[22] Postsynthetic functionalization of MOF-74 with ED can efficiently improve adsorption capacity, regeneration, and binding energies for CO_2 and other small gas molecules, e.g., CO, CO_2, SO_2, C_2H_4, NO, as well.[19,24] Hong and co-workers functionalized Mg_2(dondc) with different types of N-based molecules and showed that the CO_2 adsorption mechanism on functional groups is based on the combination of physisorption and chemisorption. The basicity of the free amine groups grafted onto the open metal sites contributes to the CO_2 uptake and most important to a better separation of CO_2 from N_2 than in pristine material.[26] Hu and co-workers confirmed that also the weight of alkylamine, the free space in MOF pores (accessibility of alkylamine), and the number and type of amine group synergistically affect the final performance of CO_2 adsorption.[23]

Among many MOF representatives, HKUST-1 (Cu(II) benzene-1,3,5-tricarboxylate) is still considered to be one of the most promising adsorbents for CO_2 capture due to its high surface area, simple and low-cost synthesis, and high density of active metal sites, which can be effectively functionalized postsynthetically.[5] Various molecular species were already used for incorporation within the HKUST-1 structure in order to improve different CO_2 capture performance parameters, for instance, incorporation of CuCl to enhance CO/H_2 and CO/N_2 separation,[27] modification with pyrazine to improve CO_2/CH_4 selectivity,[28] with *N*,*N*-dimethylformamide[29] and polyethylenimine to enhance CO_2 adsorption[30] and separation[31] or with tetraethylenepentamine for CO_2 adsorption under postcombustion conditions.[32] However, the modification of HKUST-1 with ethylenediamine to improve the CO_2 capture performance of HKUST-1 adsorbent has never been studied yet.

Herein, we present postsynthesis incorporation and detailed structural evaluation of ethylenediamine within the HKUST-1 framework for the first time. Optimization of framework-to-CO_2 binding energies, CO_2/N_2 capture selectivity, and adsorption kinetics was achieved by the incorporation of different ethylenediamine loadings.

EXPERIMENTAL SECTION

Materials. Copper(II) nitrate trihydrate (Fluka 99.9%), 1,3,5-benzene tricarboxylic acid (Sigma-Aldrich, 95%), *N*,*N*-dimethylformamide (Sigma-Aldrich, 99.9.%), methanol (Honeywell, 99.9%), toluene (Honeywell, 99.9%), ethanol (Merck, 99.9%), ethylenediamine (Sigma-Aldrich; 99%), carbon dioxide (Messer, 99.999%), and nitrogen (Messer, 99.999%) were used as purchased without further purification.

Synthesis. HKUST-1 was synthesized according to the procedure reported by Yang et al.[33] Typically, 2.0 g of copper(II) nitrate trihydrate was dissolved in 15 mL of dionized water. To this solution, 1.0 g of 1,3,5-benzenetricarboxylic acid dissolved in a mixture of 15 mL of ethanol (EtOH) and 15 mL of *N*,*N* dimethylformamide (DMF) was slowly added during continuous stirring. The reaction mixture was then transferred into a Teflon-lined stainless steel autoclave and heated at 100 °C for 12 h. After cooling to ambient temperature, blue crystals of HKUST-1 were filtered and washed with DMF twice. To extract solvent molecules from the pores, HKUST-1 was immersed in 15 mL of methanol (MeOH), which was decanted and replaced with fresh solvent every 3 h over the next 2 days. The final product was then separated by filtration and dried under a vacuum at 25 °C for 2 h and at 60 °C for 8 h.

Postsynthetic Functionalization. Before the framework functionalization, HKUST-1 was degassed under a vacuum at 150 °C for 16 h, to remove solvent molecules, thus making Cu^{2+} Lewis acid centers directly accessible for the binding of amino moieties.

Functionalization with ethylenediamine (ED) was performed using three different Cu/ED molar ratios −0.07, 0.14, and 0.3, respectively, which were chosen according to the calculated occupancy of Cu^{2+} metal centers with amine molecules. At the molar ratio of 0.07, one ED molecule theoretically occupies every 14th Cu^{2+} center, at 0.14 at every seventh, and at the molar ratio of 0.3, one ED molecule is occupies 1/3 of the Cu^{2+} center.

For functionalization, 5 μL, 10 μL, or 20 μL of ED were dissolved in 50 mL of toluene. Suspensions were added to 0.20 g of activated HKUST-1 and stirred for 4 h under reflux at 50 °C. The functionalized product was decanted and dried at room temperature overnight. In further text, modified materials were denoted as HKUST-1−5ED, HKUST-1−10ED, and HKUST-1−20ED corresponding to Cu/ED ratios of 0.07, 0.14, and 0.30 respectively.

Methods. Powder XRD data of as-synthesized and all functionalized materials were collected on a PANalytical X'Pert PRO diffractometer using CuKα radiation (λ = 1.5418 Å) at room temperature in an angular range of 5−50° (2θ) with a step size of 0.034° per 100 s using a fully opened 100 channel X'Celerator detector. The information about thermal stability of investigated samples was obtained by thermogravimetric measurements performed on a TA Instruments Q5000. The measurements were carried out in an airflow of 20 mL/min, by heating samples from 25 to 500 °C at a rate of 2 °C min^{-1}.

The Cu^{2+} concentration within the ethylenediamine-containing solution after the modification process was determined by inductive-coupled plasma atomic emission spectrometry on an Atom Scan 25 (Thermo Jarrell Ash) ICP-AES spectrometer.

N_2 sorption isotherms were measured at −196 °C on Quantachrome AUTOSORB iQ3. Before the measurement, samples were activated under a vacuum at 150 °C for 16 h. Brunauer−Emmett−Teller (BET) specific surface area calculations were performed in p/p_o relative pressure range between 1×10^{-6} and 0.12 selected according to Roquerol plots. Morphological properties of the materials were examined using Zeiss FEG SEM SUPRA 35 VP.

Fourier Transform Infrared (FTIR) spectra were recorded on a PerkinElmer Spectrum Two FT-IR spectrometer. The spectra were acquired on the powder samples with KBr addition and plotted in the 4000−400 wavenumber region.

Raman measurements have been acquired with a Bruker Senterra μ-Raman spectrometer, using a laser diode working at λ = 532 nm, a resolution of 9−15 cm^{-1} and the power of the laser set at 0.2 mW. During the measurements, the samples were kept in the air on a laboratory slide. The spectra were normalized by the intensity of the peak at 1006 cm^{-1}. Electron paramagnetic resonance (EPR) measurements were performed using a Bruker EMX micro-spectrometer working at a frequency of about 9.5 GHz (X-band) at temperatures of 77 and 300 K. The spectra were acquired using a Dewar flask containing the EPR glass tube with the sample. Only for measurements at 77 K, the Dewar flask was filled with liquid nitrogen. The spectra reported were normalized for experimental parameters and the mass of the samples. X-ray absorption near edge structure (XANES) and extended X-ray absorption fine structure (EXAFS) spectra at Cu K-edge (8979 eV) were measured on activated HKUST-1 and all functionalized materials in transmission detection mode at the XAFS beamline of the ELETTRA synchrotron radiation facility in Trieste, Italy. A Si(111) double crystal monochromator was used with an energy resolution of about 1 eV at 9 keV. Higher harmonics were eliminated by detuning of the second monochromator crystal to 60% of the maximum in the rocking curve. The intensity of the monochromatic X-ray beam was measured by three consecutive 30 cm long ionization chambers filled with optimal gas mixtures for the Cu K-edge energy range: 1250 mbar N_2, 750 mbar He (first); 250 mbar Ar, 1000 mbar N_2 750 mbar He (second); 1000 mbar N_2, 300

https://dx.doi.org/10.1021/acs.cgd.0c00667
Cryst. Growth Des. 2020, 20, 5455−5465

mbar He, 700 mbar Ar (third). The samples were prepared in the form of homogeneous pellets, pressed from micronized powder mixed with micronized BN, with a total absorption thickness of about 2 above the Cu K-edge, and inserted in the monochromatic beam between first two ionization detectors. The exact energy calibration was established with simultaneous absorption measurement on a 7 μm thick Cu metal foil, placed between the second and the third ionization chamber. Absolute energy reproducibility of the measured spectra was ±0.03 eV. The absorption spectra were measured in the energy region from −150 eV to +1100 eV relative to the Cu K-edge. Equidistant energy steps of 0.3 eV were used in the XANES region, while for the EXAFS region equidistant k steps of 0.03 Å^{-1} were adopted, with an integration time of 2 s/step. The quantitative analysis of XANES and EXAFS spectra is performed with the Demeter (IFEFFIT) program package,[34] in combination with the FEFF6 program code[35] for ab initio calculation of photoelectron scattering paths.

The X-ray photoelectron spectroscopy (XPS) analyses were carried out on the TFA XPS spectrometer produced by Physical Electronics, USA. The analyzed area was 0.4 mm in diameter, and the analyzed depth was about 3−5 nm. Sample surfaces were excited by X-ray radiation from a monochromatic Al source at a photon energy of 1486.6 eV. During data processing, the spectra from the surface were aligned by setting the C 1s peak at 284.8 eV, characteristic for C−C bonds. The accuracy of binding energies was about ±0.3 eV. Quantification of surface composition was performed from XPS peak intensities taking into account relative sensitivity factors provided by the instrument manufacturer.[36] Two different XPS measurements were performed on each sample, and the average composition was calculated.

CO_2 sorption capacities and kinetic measurements were monitored on a manometric gas analysis system HTP-IMI Hiden Isochema Inc. Before the measurement, the samples were outgassed at 150 °C for 12 h. Isosteric heats of adsorption calculations were based on sorption isotherms measured up to 1 bar at 20, 25, and 30 °C, fitted with the Toth isotherm model and using the Clausius−Clapeyron equation.[37,38] The CO_2/N_2 adsorption IAST selectivity was calculated using the Langmuir adsorption model at different partial pressures of CO_2.[39]

RESULTS AND DISCUSSION

Structure Evaluation. The efficiency of the ED incorporation within the HKUST-1 framework and effect on its structural properties were thoroughly investigated by different techniques. First comparison of powder X-ray diffraction (PXRD) patterns shown in Figure 1 indicates that after the ED modification HKUST-1 framework is preserved without any significant change of its crystallinity. Furthermore, only a slight decrease of the unit cell volumes of all modified structures in comparison with the pristine structure is expected due to the rigidity of the Cu-BTC framework (for approximately 0.1%, see Table 1 in Supporting Information). However, more detailed observations of the characteristic HKUST-1 reflections show a broadening and decrease of the intensities that are both consistently pronounced with the increase of the incorporated ED. This is the indication that the overall structural disorder is increasing with the added amount of ED. The comparison of the measured peak shape and intensities is used as an example on the (222) reflection shown in Figure S1.

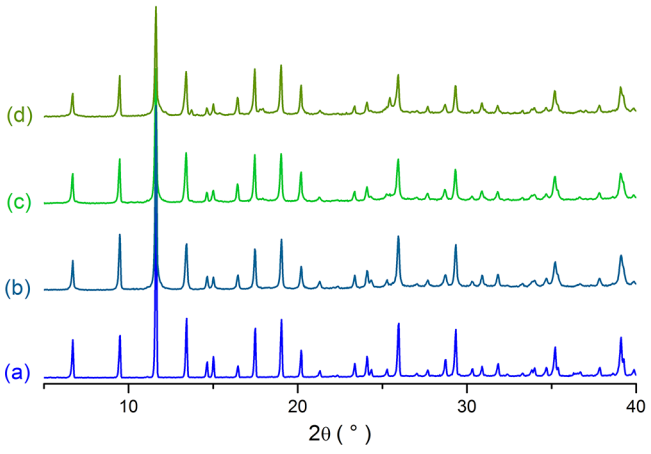

Figure 1. Powder XRD patterns of pristine HKUST-1 (a), HKUST-1−5ED (b), HKUST-1−10ED (c) and HKUST-1−20ED (d).

Additional information about the materials' content and their thermal behavior can be provided by thermogravimetric analysis (Figure 2). Nonmodified HKUST-1 show two well-separated weight losses attributed to the solvent and metal-coordinated water removal up to 150 °C followed by the framework decomposition in the narrow temperature range starting at approximately 300 °C. Between these processes, there is no other weight loss visible. Modified materials, on the other hand, show an additional weight loss between 180 and 260 °C becoming increasingly pronounced with the amount added due to the removal of additional organic moieties, which are apparently present within the modified materials. This process is more clearly visible on differential plots shown in the inset of Figure 2. From the weight losses in this specific temperature range, the amounts of incorporated ethylenediamine can be estimated to be 1.8, 2.6, and 3.1 wt % resulting in Cu/ED ratios of 0.06, 0.09, and 0.10 for HKUST-1−5ED, HKUST-1−10ED, and HKUST-1−20ED, respectively. These results imply that efficiency of ED loading is the highest for HKUST-1−5ED containing approximately 85% of the loaded amine. The incorporation efficiency gradually decreases with the loading, so the HKUST-1−10ED contains around 60% and HKUST-1−20ED only about 30% of the added ethylenediamine.

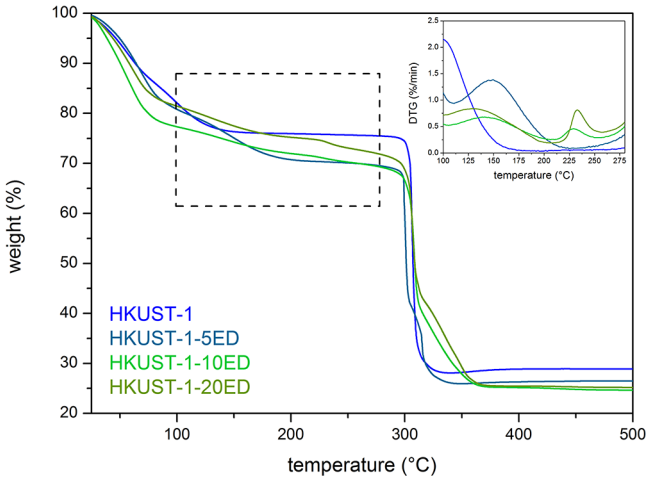

Figure 2. Thermogravimetric curves of pristine and modified HKUST-1 materials. Inset shows derivative gravimetric plots in the selected temperature range indicated by dashed square.

The effect of ED modification on HKUST-1 textural properties was evaluated by N_2 sorption isothermal measurements. Figure 3a shows a comparison of N_2 sorption isotherms of pristine HKUST-1 with the modified materials performed at 77 K, Figure 3b corresponding NLDFT pore size distribution

https://dx.doi.org/10.1021/acs.cgd.0c00667
Cryst. Growth Des. 2020, 20, 5455−5465

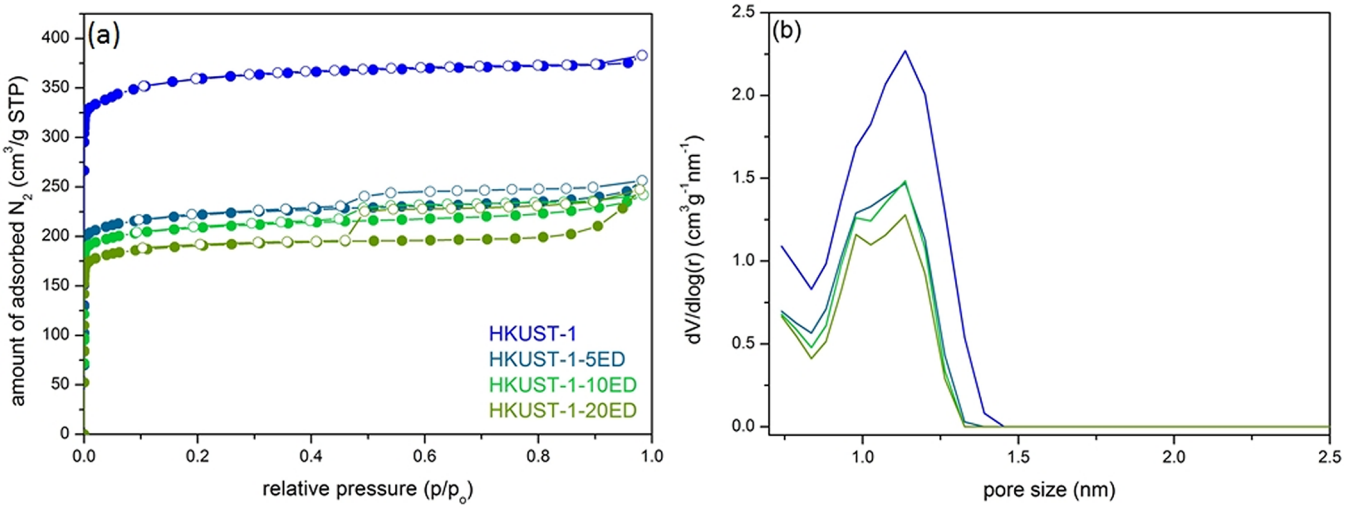

Figure 3. (a) N_2 isotherms of pristine and modified HKUST-1 materials measured at 77 K; (b) NLDFT pore size distributions of pristine and modified HKUST-1 materials.

Table 1. Textural Parameters of HKUST-1 samples

sample	S_{BET} [a] (m^2/g)	V_t [b] (cm^3/g)	V_{mic} [c] (cm^3/g)	V_{mes} [d] (cm^3/g)	V_{mes}/V_{mic}	d [e] (nm)
HKUST-1	1409	0.593	0.563	0.030	0.05	1.09
HKUST-1−5ED	881	0.398	0.349	0.049	0.14	1.05
HKUST-1−10ED	838	0.344	0.331	0.063	0.19	1.04
HKUST-1−20ED	762	0.421	0.328	0.092	0.28	1.04

[a]Specific surface area was determined from BET analysis. Selected region of relative pressures for BET calculations was based on Roquerol plots. [b]Total pore volume selected from a single adsorption point at $p/p_o = 0.99$. [c]Micropore volume calculated from t-plots. [d]Mesopore volume defined as a difference between V_t and V_{mic}. [e]Average micropore diameter determined from NLDFT pore size distribution profiles.

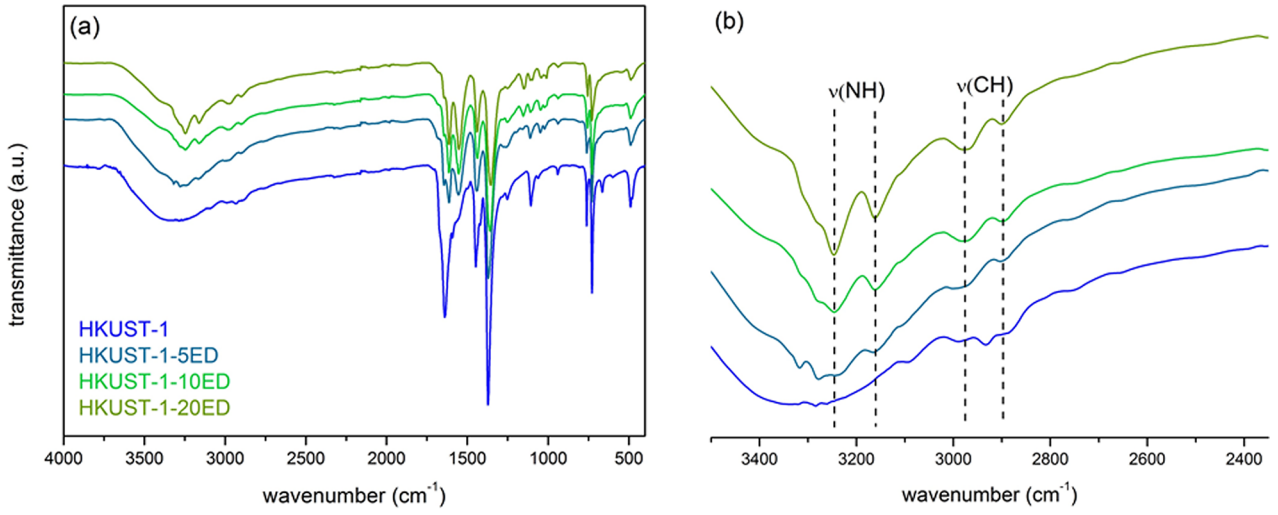

Figure 4. (a) FTIR spectra of pristine as-synthesized and modified HKUST-1 materials; (b) FTIR spectra zoomed in the selected region of wavenumbers. Dashed lines indicate bands corresponding to C−H and N−H bond vibrations respectively.

in micropore region, whereas selected textural property parameters deduced from isothermal data are collected in Table 1. Pure HKUST-1 shows a typical type-I isotherm revealing its microporous nature with the BET surface area of 1409 m^2/g, which is consistent with the literature data.[4] Modification with the smallest amount of ED (HKUST-1−5ED) already significantly decreases the specific surface area to 881 m^2/g, which further decreases with the increased amount of the added ED and contributes to the pore narrowing as well. Modified materials also show a slight increase in N_2 uptake at relative pressures close to $p/p_o = 1$, and the hysteresis of the desorption branch becomes increasingly pronounced with the increased amount of added ED. The increasing contribution of mesopores is evident from the pore volume calculations (Table 1). Mesopore volume values are calculated as the difference between total and micropore volumes, which are determined from the single point value at $p/p_o = 0.99$ and t-plot analysis, respectively. Mesopore/micropore volume ratios informatively show that pristine HKUST-1 possess a negligible amount of mesopores, whereas in the case of HKUST-1−20ED the

https://dx.doi.org/10.1021/acs.cgd.0c00667
Cryst. Growth Des. 2020, 20, 5455−5465

contribution of mesopores represents almost 30% of the total pore volume. The trend of increasing N_2 uptake close to p/p_o = 1 also implies that cavities within the HKUST-1 crystallites caused by ED modification process can reach the dimensions in the macropore region as well. The occurrence of indicated macro-/mesoporosity was additionally explored by SEM observations (Figure S2), showing that the shape of the crystallites is indeed changing significantly with the ED addition. The highest amount of added ethylenediamine causes the formation of additional openings within the crystals with the size up to 1 μm and thus establishes hierarchical structures expanded over the micro-, meso-, and macropore range.

The ED modification process apparently causes etching of the crystal surface most likely as a consequence of the HKUST-1 being exposed to basic solution causing partial dissolution of the MOF framework. This was also confirmed by the detection of Cu^{2+} cations within the ED-containing solution after the modification process. For the case of HKUST-1−20ED with the highest amount of ethylenediamine in the solution, 1.3 wt % of Cu^{2+} was leached out of the framework as determined by ICP-OES. A substantial amount of meso- and macropores within the crystal establish the micro-meso-macropore system, which can be on the other hand beneficial for the diffusion and kinetics of CO_2 adsorption.[40]

The above-described characterization methods provided information on overall changes of framework structure and porosity properties after the modification process. To get more detailed insights into the location of ED within the HKUST-1 framework and its effect on the local environment of metal centers, several spectroscopic techniques were employed further on. FT-IR spectra of the pristine and modified HKUST-1 materials are shown oin Figure 4a. Most distinctive changes in IR spectra features of pristine and modified materials, however, can be deduced in the wavenumber range around 3000 cm^{-1} (Figure 4b). In the spectra of all ED-modified HKUST-1, materials bands at 2979 and 2897 cm^{-1} are visible and can be assigned to C−H bond stretching of the aliphatic CH_2 group. These bands are less apparent on the spectrum of pure HKUST-1. Instead, it shows more intensive band at 1930 cm^{-1}, which most likely corresponds to aliphatic C−H bands originated from the DMF molecules occurring within the HKUST-1 pores as a solvent. Spectra of the modified materials exhibit several additional bands at 3163 and 3245 cm^{-1} attributed to N−H stretching vibrations and at 1012 cm^{-1} attributed to C−N vibrations, with their intensities being consistently increasing with the increasing loading of ED within the MOF matrix. The described bands in the 3100−3400 cm^{-1} region resonate at significantly lower wavenumbers as in the case of free ED with typical vibrations at 3245 and 3380 cm^{-1},[41] which can be also indicated in the spectra of the modified materials mainly as shoulders. High vibrational shift toward higher energies suggests that ED moieties are mainly bonded to free metal sites via NH_2 groups, whereas shoulders at lower energies imply the presence of free ethylenediamine within the pores as well.

Figure 5 shows Raman spectra of the ED-modified HKUST-1 materials compared to the pristine MOF. The spectrum of pristine HKUST-1 shows its characteristic bands, well-established in the literature.[42−45] Among the spectra of the pristine and modified materials, some relevant differences are recognizable. First of all, at the highest concentration of ED

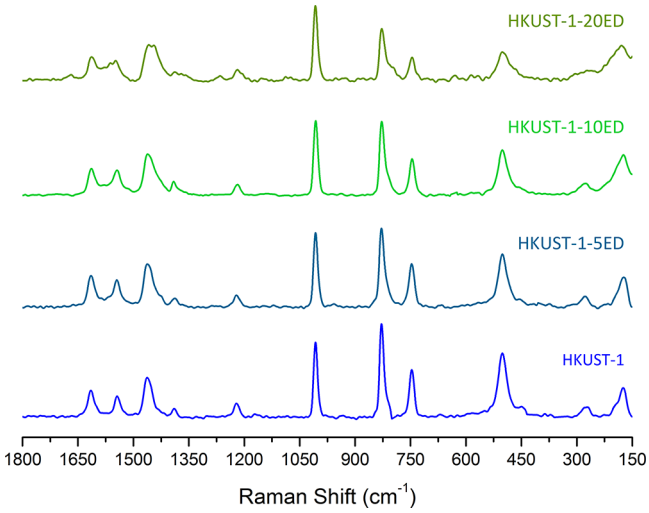

Figure 5. Comparison of Raman spectra of pristine HKUST-1 with the ED-modified materials.

(HKUST-1−20ED), new vibrational modes between the bands at 1544 and 1616 cm^{-1} have weakly emerged. Furthermore, as the ED concentration increases, there is a significant increase in the ratios between the 1006 cm^{-1} band and those peaked at lower wavenumbers. Since the bands involved in such changes arise from the Cu−O vibrational modes of the paddlewheels and of the C−H groups of the benzene rings,[42,46−48] Raman measurements suggest significant changes involving both the paddlewheel units and the organic scaffold, indicating that the introduction of the ED can produce measurable modifications of the main proprieties of the crystal.

Figure 6 shows the EPR spectra of pristine HKUST-1 and of the samples treated with ED acquired at 300 K (a) and 77 K (b). The EPR spectrum of pristine HKUST-1 obtained at 300 K shows its characteristic large and unresolved signal arising from the antiferromagnetic coupling established by the Cu^{2+} pairs of the paddle wheels.[42,47−49] Also at 77 K, the spectrum of HKUST-1 is comparable to those shown in the literature, showing signals at about 12 and 480 mT due to coupled Cu^{2+} pairs and another signal at about 330 mT arising from the Cu^{2+} extra-framework synthesis defects.[42,46−48] The introduction of the ED induces considerable changes in the EPR spectra. In fact, at both temperatures, as the ED concentration increases, the growth of a considerably strong signal is observed at the center of the spectrum, with a very similar line shapes. These features may reasonably indicate that, as a consequence of the presence of ED, a part of the paddle wheels loses the antiferromagnetic coupling of the two Cu^{2+} ions, and, as a consequence, they act as noninteracting spins. Anyway, the presence of the resonances at 12 and 480 mT proves that there still are large parts of the material with undamaged paddle wheels. In summary, the EPR data suggest that the introduction of ED within HKUST-1 induces a relevant reduction of the symmetry of the material, which significantly affects its magnetic properties. Such an effect gradually increases on increasing the content of ED.

Cu K-edge XANES analysis is used to reveal differences in the chemical state and local symmetry of Cu cations in the activated HKUST-1 and the samples after the functionalization. Normalized Cu K-edge XANES spectra of the samples, together with the spectra of corresponding Cu reference

https://dx.doi.org/10.1021/acs.cgd.0c00667
Cryst. Growth Des. 2020, 20, 5455−5465

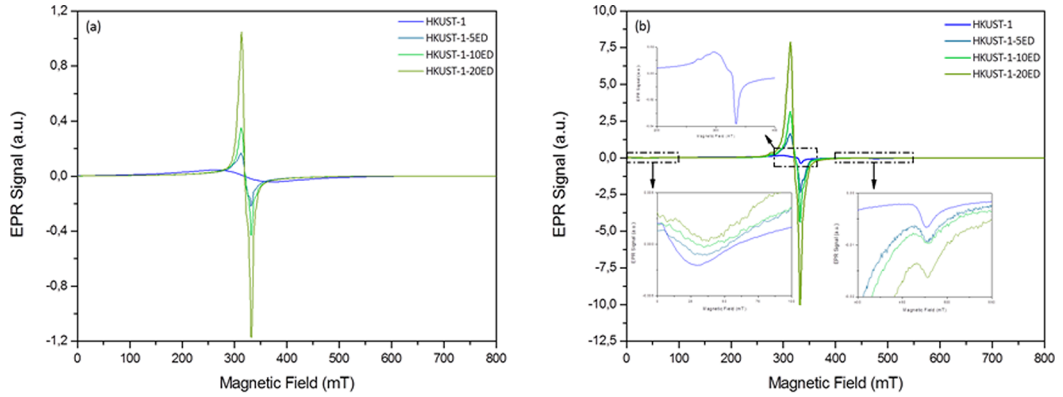

Figure 6. EPR spectra of HKUST-1 powders with different concentrations of ED at (a) 300 K and (b) 77 K.

compounds, are shown on Figure 7a. The energy position of Cu K-edge is the same in all samples and coincides with the

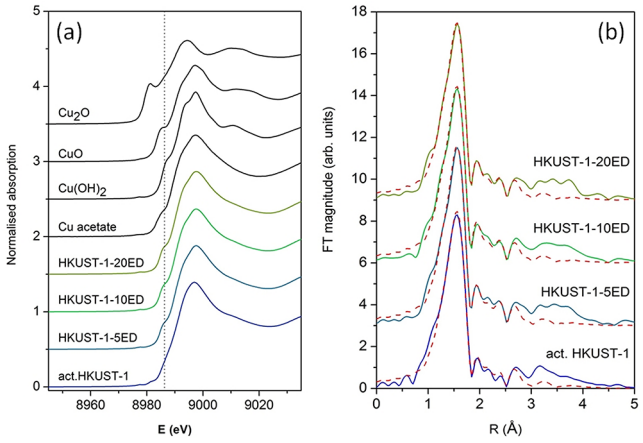

Figure 7. (a) Cu K-edge XANES spectra measured on the activated HKUST-1 sample and the functionalized HKUST-1−5ED, HKUST-1−10ED, and HKUST-1−20ED. XANES spectra of reference Cu(I) and Cu(II) compounds (Cu_2O, CuO, Cu hydroxide $(Cu(OH)_2$, and Cu acetate) are plotted for comparison. Vertical dashed line is plotted at the position of the Cu 1s-4p pre-edge absorption feature (8986 eV) in HKUST-1 samples. (b) Fourier transform magnitude of k^3-weighted Cu EXAFS spectra of the activated HKUST-1 sample and HKUST-1−5ED, HKUST-1−10ED and HKUST-1−20ED, calculated in the k range of 3−16 $Å^{-1}$ and R range of 1−3 Å. Experiment − (solid line); model -- (dashed line). Spectra are shifted vertically for clarity.

edge position of Cu^{2+} reference compounds, confirming that all Cu^{2+} cations in the samples are in divalent form, as expected for crystal structure of HKUST-1.[44] The comparison of the Cu K-edge profiles of the HKUST-1 samples clearly indicates small differences in the local symmetry of Cu^{2+} cations between the activated HKUST-1 sample compared to the ED functionalized HKUST-1 samples, while all three functionalized samples HKUST-1−5ED, HKUST-1−10ED, and HKUST-1−20ED exhibit an identical edge profile. The pre-edge shoulder at 8986 eV, characteristic for HKUST-1, that can be attributed to the 1s to 4p dipole excitation,[44] is more pronounced in the case of functionalized samples.

The structural change on the Cu site can be attributed to the coordination of the amino group of the ED to the Cu^{2+} cations in the HKUST-1 framework during the ED functionalization. The structural change does not depend on the ED loading. To identify the nature of the structural differences, we used Cu K-edge EXAFS analysis. Cu K-edge EXAFS analysis is used to probe the average local structure around Cu cations in the activated HKUST-1 and all functionalized materials. In Fourier transform magnitude of the EXAFS spectra (Figure 7b), the contributions of photoelectron scattering on the nearest shells of neighbors around the Cu atoms are observed. Qualitative comparisons of the EXAFS spectra show a small difference in the average Cu neighborhoods between the pristine HKUST-1 and functionalized samples. The EXAFS spectra of all three functionalized samples (HKUST-1−5ED, HKUST-1−10ED and HKUST-1−20ED) are identical, indicating that there are no structural differences between the samples with different ED loadings. The comparison of EXAFS spectra is consistent with XANES results.

Structural parameters of the average local Cu neighborhood (type and average number of neighbors, the radii and Debye−Waller factor of neighbor shells) are quantitatively resolved from the EXAFS spectra by comparing the measured EXAFS signal with a model signal, constructed ab initio with the FEFF6 program code.[35] The FEFF model is based on the structure of the hydrated $[Cu_2C_4O_8](H_2O)_2$ paddlewheel cluster determined by XRD on the crystal structure of HKUST-1.[44] Cu^{2+} cations in the cluster form dimers, where each Cu atom is coordinated by four oxygens at 1.96 Å, and by one water molecule at 2.19 Å in the nearest coordination shell. The Cu−Cu distance in the dimer is 2.64 Å. In next coordination shell, each Cu is coordinated to four carbon neighbors at 2.88 Å and four oxygen neighbors at 3.05 Å, belonging to the four carboxyl groups of the benzene-1,3,5-tricarboxylate ligand, connecting the Cu dimer cluster. The FEFF model comprised five single scattering and all significant multiple scattering paths up to 3.9 Å with 14 variable parameters: coordination shell distance (Δr) and the Debye−Waller factors of all single scattering paths, a separate Debye−Waller factor for multiple scattering paths, and the amplitude reduction factor S_0^2 and the shift of energy origin of the photoelectron ΔE_o, common to all scattering paths. The shell coordination numbers were fixed to the crystallographic values, except the coordination number of the O or N neighbor at 2.19 Å is varied, to detect the presence of coordinated water molecule in the activated HKUST-1 or nitrogen from coordinated amino group of the ED. The atomic species of neighbors are identified in the fit by their specific scattering factor and phase shift. However, it should be pointed out that with EXAFS analysis it is not possible to distinguish between O

https://dx.doi.org/10.1021/acs.cgd.0c00667
Cryst. Growth Des. 2020, 20, 5455−5465

Table 2. Parameters of the Nearest Coordination Shells around Cu Cations in the Activated HKUST-1 and All Modified Materials: Average Number of Neighbor Atoms (N), Distance (R), and Debye-Waller Factor (σ^2)[a]

	N		R [Å]		σ^2 [Å^2]		ΔE_o/R-factor	
Cu neigh.	HKUST-1	HKUST-1 −5,10,20ED	HKUST-1	HKUST-1− 5,10,20ED	HKUST-1	HKUST-1− 5,10,20ED	HKUST-1	HKUST-1 −5,10,20ED
O	4	4	1.963(2)	1.963(1)	0.006(1)	0.006(1)	1 ± 1 eV 0.007	3 ± 1 eV 0.005
N		0.3(1)		2.20(2)		0.006(1)		
Cu	1	1	2.64(1)	2.64(1)	0.008(1)	0.008(1)		
C	4	4	2.85(1)	2.85(1)	0.006(1)	0.006(1)		
O	4	4	3.10(5)	3.10(5)	0.03(1)	0.03(1)		

[a]Uncertainty of the last digit is given in parentheses. A best fit is obtained with the amplitude reduction factor $S_0^2 = 0.95 \pm 0.04$. The shift of the energy origin ΔE_o and R-factor (quality of fit parameter), are listed in the last column.

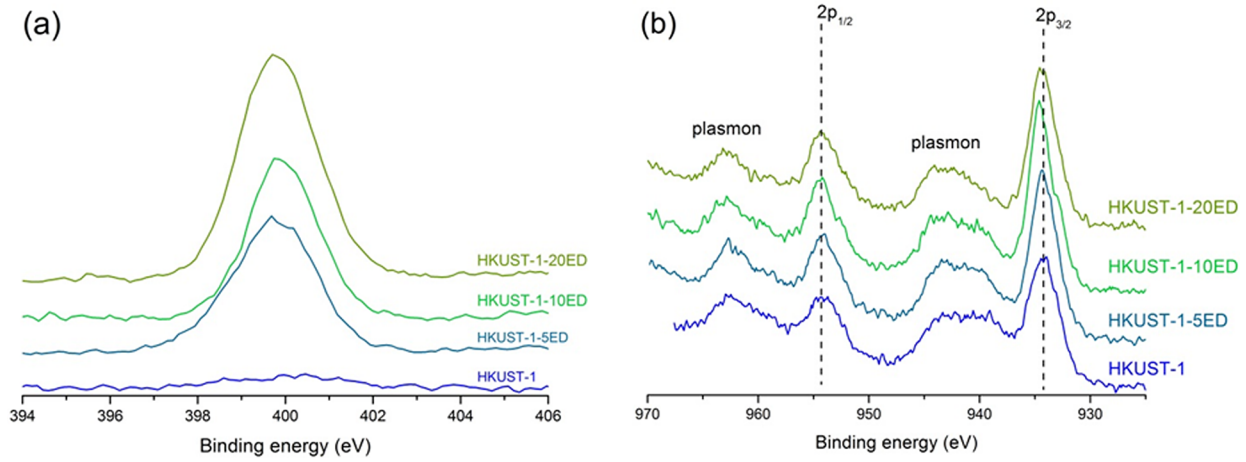

Figure 8. XPS spectra of (a) N1s and (b) Cu2p regions.

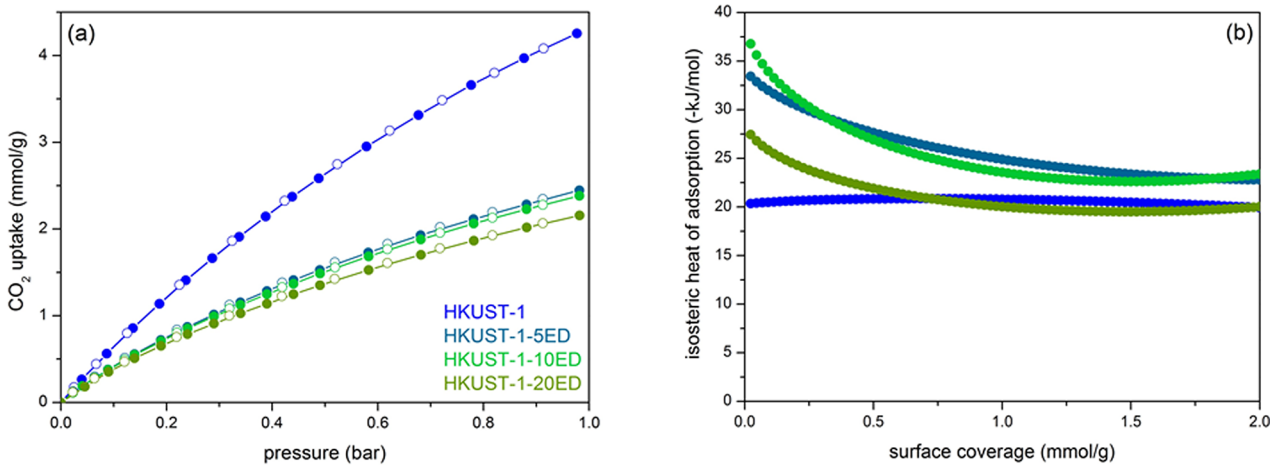

Figure 9. (a) CO_2 isotherms of pristine and modified HKUST-1 materials measured at 25 °C. Closed symbols depict adsorption points, whereas open symbols represent desorption points. (b) Isosteric heat of adsorption of pristine and modified HKUST-1 materials based on Clausius-Clayperon calculations.

and N as neighbors due to the close similarity of their scattering factor and phase shifts.

To detect small structural differences in the local Cu neighborhood between the samples, indicated also by XANES analysis, and to minimize the uncertainties of fitting parameters because of correlations between them in the fit of individual spectra, a parallel fit of the spectra was performed, in which the variable parameters for all spectra were constrained to common values, except the coordination number of O or N neighbors at 2.2 Å is varied for each sample separately. In this way, very good and stable EXAFS fits (Figure 7b) are obtained in the R-range of 1.0−3.2 Å and in the k range of 3−16 Å^{-1}. Best fit parameters are listed in Table 2.

The quantitative EXAFS results confirm the observations obtained by qualitative comparison of Cu XANES and EXAFS spectra. The average local structure around Cu^{2+} cations is the same for all three functionalized samples (HKUST-1−5ED, HKUST-1−10ED and HKUST-1−20ED), independent of the Cu/ED molar ratios, and slightly different from the spectrum of the activated HKUST-1. In all samples, we found that Cu^{2+}

https://dx.doi.org/10.1021/acs.cgd.0c00667
Cryst. Growth Des. 2020, 20, 5455−5465

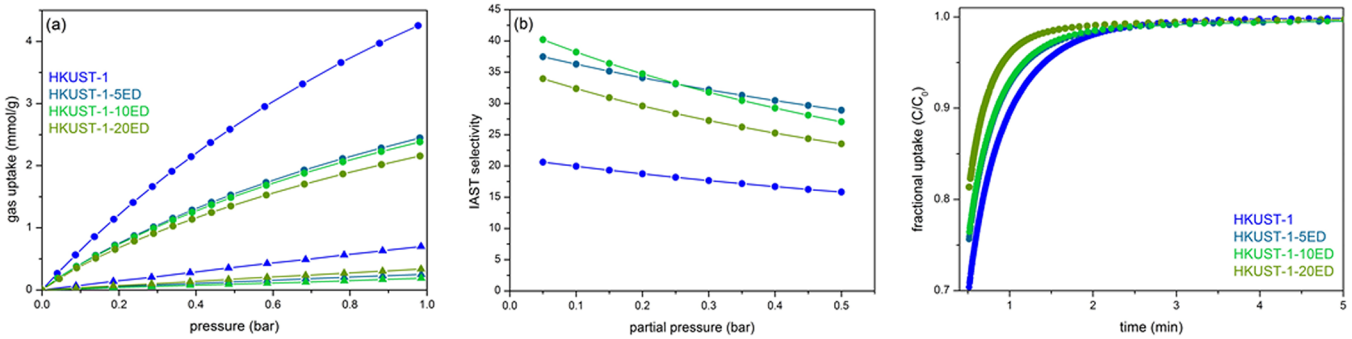

Figure 10. (a) Isotherms measured at 25 °C up to 1 bar for CO_2 (circles), N_2 (triangles), (b) IAST CO_2/N_2 selectivity as a function of CO_2 partial pressure and (c) adsorption kinetics of CO_2 dosing to 1 bar at 25 °C of pristine and modified HKUST-1 materials.

cations are bound in Cu dimer cluster characteristic for HKUST-1.[44] All structural parameters of the Cu dimer cluster (interatomic distances, coordination numbers, and Debye–Waller factors) agree with previous observations.[44] The only structural difference between pristine and functionalized samples is the coordination of nitrogen neighbor at 2.20 Å. In all three samples, we found that on average 0.3 ± 0.2 Cu^{2+} cations are coordinated to nitrogen neighbors at 2.20 Å, while in the as-synthesized material this Cu coordination site is empty.

The Cu–N bond in all functionalized samples can be ascribed to the amino group of the ED coordinated to the HKUST-1 framework. The results show that amount of directly coordinated ED to HKUST-1 framework is not increasing with the increasing loading of ED. The saturated coordination of ED to the framework is reached already at the lowest loading at the Cu/ED molar ratios of 0.07. The remaining Cu sites in the activated framework are not accessible for ED molecules.

In order to gain additional clarification about the nature of ED bonding to Cu^{2+} centers of HKUST-1 framework, XPS measurements on the investigated samples were performed as well. Figure 8a shows XPS survey spectra in N 1s region where the peak is absent for the parent HKUST-1, whereas its intensity is increasing with the increased loading of ethylenediamine. Figure 8b presents XPS spectra in Cu binding energies region showing $Cu2p_{1/2}$ and $Cu2p_{3/2}$ peaks with corresponding plasmons. Parent HKUST-1 shows an intense $Cu2p_{3/2}$ peak at a binding energy of 934.2 eV and shakeup satellites centered at approximately 940 and 943 eV, indicating an intrinsic Cu(II) state of metal cations within the structure.[50−53] The spectra of modified samples do not show any significant shifts of the binding energies, which implies that the oxidation state of Cu remains unchanged during the ED-modification process.

CO_2 Capture Performances. The effect of ED modification of HKUST-1 on CO_2 capture parameters relevant for postcombustion CO_2 was investigated. Low pressure CO_2 isotherms measured at 25 °C are represented in Figure 9a. Pure HKUST-1 exhibits the expected uptake value of 4.1 mmol/g up to 1 bar.[3] Modification with even the smallest amount of ED (HKUST-1−5ED) already decreases the CO_2 uptake 40% (2.4 mmol/g), but further deterioration is much less pronounced as the loading of ED increases. For the HKUST-1−20ED sample, the CO_2 uptake settles at 2.1 mmol/g. A similar trend was observed for the specific surface area values deduced from N_2 sorption isotherms, indicating that the CO_2 equilibrium capacity is mainly governed by the porosity or the available micropore volume within the HKUST-1 framework. The modification with the lowest amount of ED (HKUST-1−5ED) on the other hand has a significant positive effect on the isosteric heat of adsorption at low surface coverages as can be observed in Figure 9b. At zero coverage, the enthalpy of HKUST-1−5ED is enhanced from −20.3 kJ/mol to −33.4 kJ/mol with respect to pure HKUST-1. Zero coverage framework-to-CO_2 interaction continues to decrease up to −36.8 kJ/mol for HKUST-1−10ED due to the growing amount of available amine sorption sites within the MOF framework. Further loading of ED eventually inhibits the CO_2 binding energy as can be seen for the case of HKUST-1−20ED. At higher concentrations, ED does not only occupy free metal sites, but apparently, it may also be subjected to at least partial multilayer adsorption, thus blocking part of the amine sorption sites.

The ability of the modified HKUST-1 materials to selectively adsorb CO_2 from various compositions of CO_2/N_2 binary gas mixture was investigated further. Figure 10a shows single CO_2 and N_2 isothermal data from which CO_2/N_2 selectivity was determined using the IAST theory shown on Figure 10b. The trend of the separation ability with the increasing amount of incorporated ED follows the changes in isosteric heat of adsorption. At a CO_2/N_2 composition of 0.15/0.85, which is relevant for the postcombustion capture process, the selectivity is almost doubled for HKUST-1−5ED with respect to pristine HKUST-1, and it is further slightly improved for HKUST-1−10ED. The sample with the highest amount of ED (HKUST-1−20ED) on the other hand exhibits a notable deterioration of the separation ability. The tendency to adsorb CO_2 over the N_2 is greatly enhanced when a lower amount of amine sorption sites are employed within the HKUST-1 framework. With further loading of ED, the adsorption of N_2 becomes more competitive most likely due to the multilayer adsorption of ethylenediamine and gradual blocking of Lewis basic sites, which also affects the CO_2-to-framework binding energy as discussed above.

Beside the adsorption capacity and separation ability, the rapid adsorption rate is another important parameter in order to evaluate the adsorbent for real-condition capture process applications. Figure 10c shows the kinetics of CO_2 adsorption for HKUST-1 material compared to ED-modified analogues, performed with loading from a vacuum to 1 bar at 25 °C. The adsorption process is evidently faster for the modified materials, and its rate is increasing with the increasing amount of ED within the HKUST-1 framework. Adsorption kinetics is most likely related to the hierarchical porosity, which becomes increasingly emphasized with the amount of added ED as

https://dx.doi.org/10.1021/acs.cgd.0c00667
Cryst. Growth Des. 2020, 20, 5455−5465

already discussed earlier in the text. Mesoporosity generated by etching of framework structure by ED enables better accessibility and faster diffusion of CO_2 toward sorption sites.

CONCLUSIONS

HKUST-1 was structurally modified by the generation of additional amine-based sorption sites in order to investigate the impact of the modification process on CO_2 capture performances. The nature of ethylenediamine moiety binding on coordinatively unsaturated metal sites of HKUST-1 framework was evaluated by using different complementary spectroscopic techniques which strongly indicate high impact on the local structure environment even at lowest loadings of ED.

Even though the CO_2 equilibrium sorption capacity notably deteriorates after modification, the enthalpy of adsorption and CO_2/N_2 selectivity both are improved for almost 85% in the case of HKUST-1−10ED in comparison to pristine HKUST-1. Higher amounts of ED, on the other hand, have a negative effect on both parameters most likely due to the successive multilayer adsorption of ED within the HKUST-1 micropores partially blocking generated sorption sites. Modification of the HKUST-1 framework with ED causes partial degradation of crystalline framework forming microporous/mesoporous system which notably enhances the adsorption kinetics of CO_2 due to the easier diffusion through the adsorbent.

ASSOCIATED CONTENT

Supporting Information

The Supporting Information is available free of charge at https://pubs.acs.org/doi/10.1021/acs.cgd.0c00667.

XRD patterns focused on (222) reflection of HKUST-1 structure, unit cell parameters, SEM micrographs, CO_2 isotherms measured at 20, 25 and 30 °C, Cu 2p high-resolution XPS spectra with fits (PDF)

AUTHOR INFORMATION

Corresponding Author

Matjaž Mazaj − *National Institute of Chemistry, 1000 Ljubljana, Slovenia;* orcid.org/0000-0003-3196-9079; Email: matjaz.mazaj@ki.si

Authors

Nika Vrtovec − *National Institute of Chemistry, 1000 Ljubljana, Slovenia; Faculty of Chemistry and Technology, University of Ljubljana, 1000 Ljubljana, Slovenia*

Gianpiero Buscarino − *Dipartimento di Fisica e Chimica, Università di Palermo, 90123 Palermo, Italy;* orcid.org/0000-0001-8324-6783

Angela Terracina − *Dipartimento di Fisica e Chimica, Università di Palermo, 90123 Palermo, Italy;* orcid.org/0000-0002-6906-4921

Simonpietro Agnello − *Dipartimento di Fisica e Chimica, Università di Palermo, 90123 Palermo, Italy;* orcid.org/0000-0002-0346-8333

Iztok Arčon − *University of Nova Gorica, 5000 Nova Gorica, Slovenia; Jožef Stefan Institute, 1000 Ljubljana, Slovenia*

Janez Kovač − *Jožef Stefan Institute, 1000 Ljubljana, Slovenia*

Nataša Zabukovec Logar − *National Institute of Chemistry, 1000 Ljubljana, Slovenia; University of Nova Gorica, 5000 Nova Gorica, Slovenia*

Complete contact information is available at: https://pubs.acs.org/10.1021/acs.cgd.0c00667

Author Contributions

[▽]N.V. performed the synthesis work and sorption measurement experiments. M.M. and N.Z.L. contributed equally in supervision and coordination of the research work. G.B. and A.T. contributed with EPR measurements. S.A contributed with Raman experiments. I.A. performed the EXAFS/XANES analysis. J.K. performed XPS analysis.

Funding

Slovenian Research Agency Research programs P1-0021. Slovenian Research Agency Research programs J1-8146. EU Framework Programme for Research and Innovation HORIZON 2020FP CALIPSOplus under the Grant Agreement 730872. SR facilities of ELETTRA (beamline XAFS, pr. 20170045 and 20155510).

Notes

The authors declare no competing financial interest.

ACKNOWLEDGMENTS

We would like to thank Giuliana Aquilanti of ELETTRA for expert advice on beamline operation.

REFERENCES

(1) Leung, D. Y. C.; Caramanna, G.; Maroto-Valer, M. M. An Overview of Current Status of Carbon Dioxide Capture and Storage Technologies. *Renewable Sustainable Energy Rev.* **2014**, *39*, 426−443.

(2) Olajire, A. A. CO2 Capture and Separation Technologies for End-of-Pipe Applications − A Review. *Energy* **2010**, *35*, 2610−2628.

(3) Ding, M.; Flaig, R. W.; Jiang, H.-L.; Yaghi, O. M. Carbon Capture and Conversion Using Metal−Organic Frameworks and MOF-Based Materials. *Chem. Soc. Rev.* **2019**, *48*, 2783−2828.

(4) Sumida, K.; Rogow, D. L.; Mason, J. A.; McDonald, T. M.; Bloch, E. D.; Herm, Z. R.; Bae, T.-H.; Long, J. R. Carbon Dioxide Capture in Metal−Organic Frameworks. *Chem. Rev.* **2012**, *112*, 724−781.

(5) Raganati, F.; Gargiulo, V.; Ammendola, P.; Alfe, M.; Chirone, R. CO2 Capture Performance of HKUST-1 in a Sound Assisted Fluidized Bed. *Chem. Eng. J.* **2014**, *239*, 75−86.

(6) Mondal, M. K.; Balsora, H. K.; Varshney, P. Progress and Trends in CO2 Capture/Separation Technologies: A Review. *Energy* **2012**, *46*, 431−441.

(7) *Module 2 CO_2 Capture: Post Combustion Flue Gas Separation*; Global CCS Institute, https://www.globalccsinstitute.com/archive/hub/publications/29721/co2-capture-technologies-pcc.pdf (accessed Jun 7, 2018).

(8) Hu, Z.; Wang, Y.; Shah, B. B.; Zhao, D. CO_2 Capture in Metal−Organic Framework Adsorbents: An Engineering Perspective. *Adv. Sustain. Syst.* **2019**, *3*, 1800080.

(9) Siegelman, R. L.; McDonald, T. M.; Gonzalez, M. I.; Martell, J. D.; Milner, P. J.; Mason, J. A.; Berger, A. H.; Bhown, A. S.; Long, J. R. Controlling Cooperative CO2 Adsorption in Diamine-Appended Mg2(Dobpdc) Metal−Organic Frameworks. *J. Am. Chem. Soc.* **2017**, *139*, 10526−10538.

(10) Majchrzak, A.; Nowak, W. Separation Characteristics as a Selection Criteria of CO 2 Adsorbents. *J. CO2 Util.* **2017**, *17*, 69−79.

(11) Trickett, C. A.; Helal, A.; Al-Maythalony, B. A.; Yamani, Z. H.; Cordova, K. E.; Yaghi, O. M. The Chemistry of Metal−Organic Frameworks for CO2 Capture, Regeneration and Conversion. *Nat. Rev. Mater.* **2017**, *2*, 17045.

(12) Olajire, A. A. Synthesis Chemistry of Metal-Organic Frameworks for CO2 Capture and Conversion for Sustainable Energy Future. *Renewable Sustainable Energy Rev.* **2018**, *92*, 570−607.

(13) Belmabkhout, Y.; Guillerm, V.; Eddaoudi, M. Low Concentration CO2 Capture Using Physical Adsorbents: Are Metal-Organic

Frameworks Becoming the New Benchmark Materials? *Chem. Eng. J.* **2016**, *296*, 296−386.
(14) Zhang, Z.; Zhao, Y.; Gong, Q.; Li, Z.; Li, J. MOFs for CO_2 Capture and Separation from Flue Gas Mixtures: The Effect of Multifunctional Sites on Their Adsorption Capacity and Selectivity. *Chem. Commun.* **2013**, *49*, 653−661.
(15) Andirova, D.; Lei, Y.; Zhao, X.; Choi, S. Functionalization of Metal−Organic Frameworks for Enhanced Stability under Humid Carbon Dioxide Capture Conditions. *ChemSusChem* **2015**, *8*, 3405−3409.
(16) Furukawa, H.; Cordova, K. E.; O'Keeffe, M.; Yaghi, O. M. The Chemistry and Applications of Metal-Organic Frameworks. *Science* **2013**, *341*, 1230444−1230444.
(17) Millward, A. R.; Yaghi, O. M. Metal−Organic Frameworks with Exceptionally High Capacity for Storage of Carbon Dioxide at Room Temperature. *J. Am. Chem. Soc.* **2005**, *127*, 17998−17999.
(18) Álvarez, J. R.; Sánchez-González, E.; Pérez, E.; Schneider-Revueltas, E.; Martínez, A.; Tejeda-Cruz, A.; Islas-Jácome, A.; González-Zamora, E.; Ibarra, I. A. Structure Stability of HKUST-1 towards Water and Ethanol and Their Effect on Its CO2 Capture Properties. *Dalton Trans.* **2017**, *46*, 9192−9200.
(19) Tan, K.; Zuluaga, S.; Fuentes, E.; Mattson, E. C.; Veyan, J.-F.; Wang, H.; Li, J.; Thonhauser, T.; Chabal, Y. J. Trapping Gases in Metal-Organic Frameworks with a Selective Surface Molecular Barrier Layer. *Nat. Commun.* **2016**, *7*, 13871.
(20) Lin, Y.; Kong, C.; Chen, L. Amine-Functionalized Metal−Organic Frameworks: Structure, Synthesis and Applications. *RSC Adv.* **2016**, *6*, 32598−32614.
(21) Peikert, K.; Hoffmann, F.; Fröba, M. Amino Substituted Cu3(Btc)2: A New Metal−Organic Framework with a Versatile Functionality. *Chem. Commun.* **2012**, *48*, 11196.
(22) Demessence, A.; D'Alessandro, D. M.; Foo, M. L.; Long, J. R. Strong CO_2 Binding in a Water-Stable, Triazolate-Bridged Metal−Organic Framework Functionalized with Ethylenediamine. *J. Am. Chem. Soc.* **2009**, *131*, 8784−8786.
(23) Hu, Y.; Verdegaal, W. M.; Yu, S.-H.; Jiang, H.-L. Alkylamine-Tethered Stable Metal−Organic Framework for CO2 Capture from Flue Gas. *ChemSusChem* **2014**, *7*, 734−737.
(24) Choi, S.; Watanabe, T.; Bae, T.-H.; Sholl, D. S.; Jones, C. W. Modification of the Mg/DOBDC MOF with Amines to Enhance CO_2 Adsorption from Ultradilute Gases. *J. Phys. Chem. Lett.* **2012**, *3*, 1136−1141.
(25) Chen, J.; Liu, R.; Gao, H.; Chen, L.; Ye, D. Amine-Functionalized Metal-Organic Frameworks for the Transesterification of Triglycerides. *J. Mater. Chem. A* **2014**, *2*, 7205−7213.
(26) Song, F.; Zhong, Q.; Zhao, Y. A Protophilic Solvent-Assisted Solvothermal Approach to Cu-BTC for Enhanced CO_2 Capture: Protophilic Solvothermal Approach to Cu-BTC for CO_2 Capture. *Appl. Organomet. Chem.* **2015**, *29*, 612−617.
(27) Yin, Y.; Wen, Z.-H.; Liu, X.-Q.; Shi, L.; Yuan, A.-H. Modification of Metal Organic Framework HKUST-1 with CuCl for Selective Separation of CO/H_2 and CO/N_2. *J. Porous Mater.* **2018**, *25*, 1513.
(28) Salehi, S.; Anbia, M. High CO_2 Adsorption Capacity and CO_2/CH_4 Selectivity by Nanocomposites of MOF-199. *Energy Fuels* **2017**, *31*, 5376−5384.
(29) Ma, L.; Tang, H.; Zhou, C.; Zhang, H.; Yan, C.; Hu, X.; Yang, Y.; Yang, W.; Li, Y.; He, D. Carbon Dioxide Adsorption Behavior of Modified HKUST-1. *Int. J. Nanosci.* **2014**, *13*, 1460002.
(30) Irani, V.; Tavasoli, A.; Maleki, A.; Vahidi, M. Polyethyleneimine-Functionalized HKUST-1/MDEA Nanofluid to Enhance the Absorption of CO2 in Gas Sweetening Process. *Int. J. Hydrogen Energy* **2018**, *43*, 5610−5619.
(31) Aarti, A.; Bhadauria, S.; Nanoti, A.; Dasgupta, S.; Divekar, S.; Gupta, P.; Chauhan, R. $[Cu_3(BTC)_2]$-Polyethyleneimine: An Efficient MOF Composite for Effective CO_2 Separation. *RSC Adv.* **2016**, *6*, 93003−93009.
(32) Martínez, F.; Sanz, R.; Orcajo, G.; Briones, D.; Yángüez, V. Amino-Impregnated MOF Materials for CO 2 Capture at Post-Combustion Conditions. *Chem. Eng. Sci.* **2016**, *142*, 55−61.
(33) Yang, Y.; Shukla, P.; Wang, S.; Rudolph, V.; Chen, X.-M.; Zhu, Z. Significant Improvement of Surface Area and CO2 Adsorption of Cu−BTC via Solvent Exchange Activation. *RSC Adv.* **2013**, *3*, 17065.
(34) Ravel, B.; Newville, M. It ATHENA, It ARTEMIS, It HEPHAESTUS: Data Analysis for X-Ray Absorption Spectroscopy Using It IFEFFIT. *J. Synchrotron Radiat.* **2005**, *12*, 537−541.
(35) Rehr, J. J.; Albers, R. C.; Zabinsky, S. I. High-Order Multiple-Scattering Calculations of x-Ray-Absorption Fine Structure. *Phys. Rev. Lett.* **1992**, *69*, 3397−3400.
(36) Moulder, J. F.; Chastain, J.; King, R. C. *Handbook of X-Ray Photoelectron Spectroscopy: A Reference Book of Standard Spectra for Identification and Interpretation of XPS Data*; Physical Electronics, 1995.
(37) Brown, O. L. I. The Clausius-Clapeyron Equation. *J. Chem. Educ.* **1951**, *28*, 428.
(38) Gregg, S. J.; Sing, K. S. W. *Adsorption, Surface Area, and Porosity*; Academic Press: London, 1982.
(39) Simon, C. M.; Smit, B.; Haranczyk, M. PyIAST: Ideal Adsorbed Solution Theory (IAST) Python Package. *Comput. Phys. Commun.* **2016**, *200*, 364−380.
(40) Mazaj, M.; Bjelica, M.; Žagar, E.; Logar, N. Z.; Kovačič, S. Zeolite Nanocrystals Embedded in Microcellular Carbon Foam as a High-Performance CO2 Capture Adsorbent with Energy-Saving Regeneration Properties. *ChemSusChem* **2020**, *13*, 2089−2097.
(41) Segal, L.; Eggerton, F. V. Infrared Spectra of Ethylenediamine and the Dimethylethylenediamines. *Appl. Spectrosc.* **1961**, *15*, 116−117.
(42) Terracina, A.; McHugh, L. N.; Todaro, M.; Agnello, S.; Wheatley, P. S.; Gelardi, F. M.; Morris, R. E.; Buscarino, G. Multitechnique Analysis of the Hydration in Three Different Copper Paddle-Wheel Metal−Organic Frameworks. *J. Phys. Chem. C* **2019**, *123*, 28219−28232.
(43) Todaro, M.; Alessi, A.; Sciortino, L.; Agnello, S.; Cannas, M.; Gelardi, F. M.; Buscarino, G. Investigation by Raman Spectroscopy of the Decomposition Process of HKUST-1 upon Exposure to Air. *J. Spectrosc.* **2016**, *2016*, 1.
(44) Prestipino, C.; Regli, L.; Vitillo, J. G.; Bonino, F.; Damin, A.; Lamberti, C.; Zecchina, A.; Solari, P. L.; Kongshaug, K. O.; Bordiga, S. Local Structure of Framework Cu(II) in HKUST-1 Metallorganic Framework: Spectroscopic Characterization upon Activation and Interaction with Adsorbates. *Chem. Mater.* **2006**, *18*, 1337−1346.
(45) Dhumal, N. R.; Singh, M. P.; Anderson, J. A.; Kiefer, J.; Kim, H. J. Molecular Interactions of a Cu-Based Metal−Organic Framework with a Confined Imidazolium-Based Ionic Liquid: A Combined Density Functional Theory and Experimental Vibrational Spectroscopy Study. *J. Phys. Chem. C* **2016**, *120*, 3295−3304.
(46) Todaro, M.; Buscarino, G.; Sciortino, L.; Alessi, A.; Messina, F.; Taddei, M.; Ranocchiari, M.; Cannas, M.; Gelardi, F. M. Decomposition Process of Carboxylate MOF HKUST-1 Unveiled at the Atomic Scale Level. *J. Phys. Chem. C* **2016**, *120*, 12879−12889.
(47) Terracina, A.; Todaro, M.; Mazaj, M.; Agnello, S.; Gelardi, F. M.; Buscarino, G. Unveiled the Source of the Structural Instability of HKUST-1 Powders upon Mechanical Compaction: Definition of a Fully Preserving Tableting Method. *J. Phys. Chem. C* **2019**, *123*, 1730−1741.
(48) Pöppl, A.; Kunz, S.; Himsl, D.; Hartmann, M. CW and Pulsed ESR Spectroscopy of Cupric Ions in the Metal−Organic Framework Compound Cu3(BTC)2. *J. Phys. Chem. C* **2008**, *112*, 2678−2684.
(49) Todaro, M.; Buscarino, G.; Sciortino, L.; Alessi, A.; Messina, F.; Taddei, M.; Ranocchiari, M.; Cannas, M.; Gelardi, F. M. Decomposition Process of Carboxylate MOF HKUST-1 Unveiled at the Atomic Scale Level. *J. Phys. Chem. C* **2016**, *120*, 12879−12889.
(50) Chanquía, C. M.; Sapag, K.; Rodríguez-Castellón, E.; Herrero, E. R.; Eimer, G. A. Nature and Location of Copper Nanospecies in Mesoporous Molecular Sieves. *J. Phys. Chem. C* **2010**, *114*, 1481−1490.

https://dx.doi.org/10.1021/acs.cgd.0c00667
Cryst. Growth Des. 2020, 20, 5455−5465

(51) Papavasiliou, J.; Avgouropoulos, G.; Ioannides, T. Combined Steam Reforming of Methanol over Cu−Mn Spinel Oxide Catalysts. *J. Catal.* **2007**, *251*, 7−20.
(52) Espinós, J. P.; Morales, J.; Barranco, A.; Caballero, A.; Holgado, J. P.; González-Elipe, A. R. Interface Effects for Cu, CuO, and Cu_2O Deposited on SiO_2 and ZrO_2. XPS Determination of the Valence State of Copper in Cu/SiO_2 and Cu/ZrO_2 Catalysts. *J. Phys. Chem. B* **2002**, *106*, 6921−6929.
(53) Chiericatti, C.; Basilico, J. C.; Zapata Basilico, M. L.; Zamaro, J. M. Novel Application of HKUST-1 Metal−Organic Framework as Antifungal: Biological Tests and Physicochemical Characterizations. *Microporous Mesoporous Mater.* **2012**, *162*, 60−63.

https://dx.doi.org/10.1021/acs.cgd.0c00667
Cryst. Growth Des. 2020, 20, 5455−5465